CRYSTAL GROWTH & DESIGN

Article

pubs.acs.org/crystal

Epitaxially Intergrown Conformational Polymorphs and a Mixed Water/Methanol Solvate of 5′-Deoxy-5′-iodoguanosine

Sean R. Parkin,*[,†] Karl J. Thorley,[†,‡] Kevin J. Gagnon,[§] and Edward J. Behrman[∥]

[†]Department of Chemistry, University of Kentucky, Lexington, Kentucky 40506, United States

[‡]Center for Applied Energy Research, University of Kentucky, Lexington, Kentucky 40511, United States

[§]Advanced Light Source, LBNL, Berkeley, California 94720, United States

[∥]Department of Chemistry and Biochemistry, Ohio State University, Columbus, Ohio 43210, United States

Supporting Information

ABSTRACT: 5′-Deoxy-5′-iodoguanosine (**I**) crystals deposited from mixtures of water and methanol grow as nonsolvated hybrids of conformational polymorphs (**Ia**, **Ib**) and as a mixed solvate (**Ic**). Some solvent-free crystals are purely **Ia**, while others have varying amounts of **Ib** epitaxially intergrown with **Ia**. In **Ia** and **Ib** the conformations differ primarily by torsion about the C4′−C5′ bond (guanosine numbering scheme), which dramatically affects the iodine atom position. Powder diffraction and reconstructed reciprocal-lattice-slice images had small peaks incompatible with **Ia**. Some solvent-free crystals required lattices for both **Ia** and **Ib** to index all observable reflections. Unit-cell dimensions for **Ia** and **Ib** suggest the potential for epitaxial intergrowth. Hydrogen-bond networks in **Ia** and **Ib** are essentially identical and result in double layers of molecules in the *ab* plane, with layers of iodine at the layer surfaces. The iodine layers of **Ia** and **Ib** are incompatible: in **Ia** adjacent iodine atom layers interdigitate slightly, whereas in **Ib** they do not. Theoretical calculations support the conclusion that at room temperature **Ia** is the thermodynamically more stable polymorph and that **Ib** represents a kinetic product.

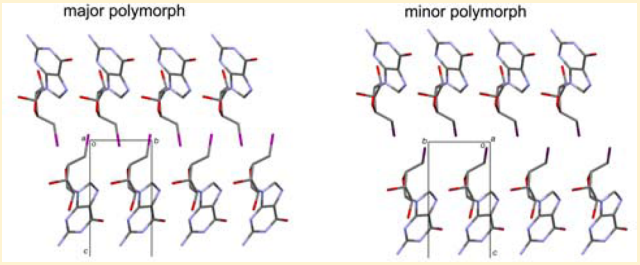

1. INTRODUCTION

Polymorphism is the well-known phenomenon in which a compound crystallizes with more than one distinct crystal structure but identical chemical composition.[1−3] Broadly speaking, there are two main types: polymorphism that results from packing differences only, and polymorphism arising from differences in molecular conformation. Crystals containing different solvents or quantities of solvent are not polymorphs but have been referred to as "solvatomorphs" and "pseudopolymorphs", though not without controversy.[4−6] Polymorphs and related solvates can have commercial ramifications in crystal engineering because changes in crystal structure, whether due to packing differences, conformational changes, or both, can lead to dramatic differences in physical properties. In the pharmaceutical industry, for example, polymorphs in drug formulations may exhibit very different dissolution properties, which can affect bioavailability. The most famous example is probably the antiretroviral drug ritonavir.[7] In the field of organic electronics, properties of crystals and crystalline thin films are critically dependent upon the manner in which electronically active functional groups on adjacent molecules interact. Even subtle changes in crystal packing can dramatically affect properties such as conductivity and electron/hole mobility.[8,9]

5′-Deoxy-5′-iodoguanosine (**I**, Scheme 1) is a versatile starting material used to produce a wide variety of 5′-deoxyguanosines[10] for use in site-specific modification of RNA.[11−13] The synthesis of **I** has been reported via several synthetic routes.[14−16] Its crystal structure, however, has thus far not been reported, perhaps as a consequence of the unusual diffraction encountered in the present study. In the course of work on substituted 5′-deoxyguanosines, we first obtained very small rectangular plate-like crystals of **I** by evaporation of MeOH from a solution in mixed H_2O/MeOH. These crystals contained two independent molecules of **I** that had quite different conformations, along with water and methanol. Subsequent crystals grown from water and or water/methanol

Scheme 1. 5′-Deoxy-5′-iodoguanosine (I)

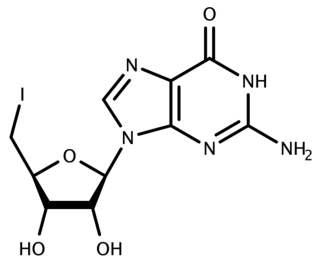

Received: June 30, 2016
Revised: October 4, 2016
Published: October 10, 2016

DOI: 10.1021/acs.cgd.6b00981
Cryst. Growth Des. 2016, 16, 6343−6353

Table 1. Crystallographic Parameters for Polymorphs Ia and Ib, and for the Mixed Water/Methanol Solvate Ic

	Ia	Ib	Ic
formula	$C_{10}H_{12}I_1N_5O_4$	$C_{10}H_{12}I_1N_5O_4$	$C_{10}H_{12}I_1N_5O_4{\cdot}3H_2O{\cdot}MeOH$[a]
formula weight	393.15	393.15	446.43[b]
temperature (K)	90.0(2)	100(2)	90.0(2)
crystal system	monoclinic	monoclinic	orthorhombic
space group	$P2_1$	$P2_1$	$P2_12_12_1$
a (Å)	7.6285(4)	7.5536(15)	9.2724(2)
b (Å)	4.9951(2)	4.9860(8)	10.5959(3)
c (Å)	16.1724(7)	17.691(3)	32.2592(8)
β (deg)	91.843(2)	102.172(1)	
volume (Å^3)	615.95(5)	651.3(2)	3168.55(14)
Z, Z'	2, 1	2, 1	8, 2
μ (mm^{-1})	6.686	20.680	16.282[b]
reflections	7526	3181	28525
unique reflections	1769	1699	5524
R_{int}	0.0379	0.0476	0.0524
final R_1 [$I > 2\sigma(I)$]	0.0229	0.0699	0.0420
$wR(F^2)$ (all data)	0.0582	0.1915	0.1093
goodness-of-fit	1.062	1.098	1.043
Flack parameter	0.019(9)	0.211(19)	0.045(4)
$\Delta\rho$ min/max (e·Å^{-3})	0.471/−0.851	1.132/−3.191	0.984/−1.068

[a]Formula does not include the diffuse feature that was modeled as partial occupancy disordered water/methanol. [b]Includes contribution from the diffuse feature that was modeled as partial occupancy disordered water/methanol.

were mostly lath-shaped and solvent free. Their structure, **Ia**, solved easily, but the diffraction pattern contained unusual features. Comparison of powder diffraction patterns for the solvent-free crystals to a powder pattern calculated from the refined single-crystal structure revealed a few small peaks in the experimental pattern that indicated the presence of a phase that did not fit either **Ia** or that of the solvate. Similarly, reciprocal-lattice-slice images calculated from a full set of raw diffraction frames revealed a small number of weak Bragg peaks that do not correspond to the structure of **Ia**. The unusual diffraction from these crystals prompted a closer look. At the Advanced Light Source (ALS, LBNL, Berkeley, CA), a miniscule squat slab-shaped crystal gave diffraction that clearly showed two different but related mutually oriented reciprocal lattices. One unit cell matched that of **Ia**, while the other was for a second polymorph, **Ib**.

Epitaxial intergrowth of polymorphs and solvates is not unknown in molecular crystals, but it is not common. Two examples of polymorphic hybrid molecular crystals are DL-homocysteine thiolactone hydrochloride[17] and aspirin,[18] but these are strictly packing polymorphs, whereas **Ia** and **Ib** are conformational polymorphs. An example of epitaxial intergrowth of anhydrous and hydrated forms with biological implications is uric acid.[19,20] In this paper we describe the structures and hydrogen bonding in polymorphs **Ia** and **Ib**, and suggest plausible reasons for the observed variable intergrowth of the two forms. For the sake of completeness, we also report the crystal structure of the mixed H_2O/MeOH solvate **Ic**.

2. EXPERIMENTAL SECTION

2.1. Synthesis and Crystallization. Synthesis of **I** followed the procedure of McGee and Martin.[14] The first crystals were produced by dissolving **I** (50 mg) in boiling methanol/water (3 mL, 1:1) and allowing the methanol to evaporate slowly at RT. The initial preparation gave crystals of the H_2O/MeOH solvate **Ic**. IR (Nujol): 3386, 3283, 3136, 1704, 1678, 1628, 1565, 1529, 1349, 1330, 1244, 1161, 1120, 1008, 941, 826, 683. Deuterated crystals were prepared by dissolving **I** (50 mg) in boiling D_2O (5 mL) and continuing the heating in a boiling water bath for 5 min. The heat source was turned off, and the solution was slowly cooled to RT. The crystals were filtered, washed with D_2O, and then either air-dried or kept wet. The resulting crystals did not contain solvent and was indexed to give cell dimensions of form **Ia**. Subsequent preparations from either methanol/water or water alone (deuterated or protonated) appeared to give only the nonsolvated crystals (i.e., **Ia** and hybrid **Ia**/**Ib**), though not all batches were subject to crystallographic analysis. IR (Nujol): 2597, 2507, 2444, 2351, 1665, 1650, 1563, 1537, 1456, 1346, 1293, 1261,1082, 1070, 1015, 958, 923, 779, 706. The ^{1}H-NMR spectrum in wet deuterated DMSO matched the data of McGee and Martin.[14]

2.2. Single-Crystal Data Collection. All crystals obtained in this work were very small. The nonsolvated crystals grew as flattened rods or laths with typical dimensions 0.15 × 0.04 × 0.01 mm, elongated along b and flattened along c, though a few were slightly longer and/or thicker (Table 1, SI Figure S1). A very few crystals were semiregular squat slabs, typically 0.04 × 0.03 × 0.01 mm. Crystals of the H_2O/MeOH solvate were rectangular plates with maximum dimension ~0.20 mm, but only ~0.005−0.010 mm thick. For analysis, crystals were submerged in a drop of polyisobutene oil, cleaned of adhering smaller crystals, and mounted on either fine glass fibers or on polyimide scoops (MiTeGen) under a polarizing microscope. Crystals of **Ia** and **Ic** were mounted directly into the 90.0(2) K cold-gas stream (CryoIndustries LT-2), and data were collected using ϕ and ω scans with Cu Kα X-rays on a Bruker-Nonius X8 Proteum diffractometer equipped with multilayer focusing optics. Diffraction data for **Ib** from a slab-shaped crystal containing both **Ia** and **Ib** were collected using ϕ and ω scans at 100(2) K (Oxford Cryosystems Cryostream 800 Plus) on beamline 11.3.1 at the ALS using a wavelength of 1.0333(1) Å on a Bruker Photon100 CMOS equipped D8 diffractometer. In all cases, raw diffraction images were integrated using Saint-Plus in APEX2.[21] Tools within APEX2 for handling twinned crystal data were used to partition reflections from **Ia** and **Ib** for separate indexing. Data scaling, merging, and absorption correction were performed using SADABS.[22] For **Ib**, a postrefinement correction using XABS2[23] was beneficial, presumably because this alleviated some residual effects of reflection overlap for the superimposed diffraction maxima of **Ia** with those of **Ib**.

2.3. Structure Solution and Refinement. Structures were solved using SHELXT[24] and refined using SHELXL.[25] In **Ia**, all hydrogen atoms were found in difference maps. Hydrogens attached to carbon or oxygen were included using riding models, but those of the

DOI: 10.1021/acs.cgd.6b00981
Cryst. Growth Des. 2016, 16, 6343−6353

exocyclic amine were refined. In **Ib**, carbon-bound hydrogens were found in difference maps, but those bound to nitrogen or oxygen were placed at calculated positions: all were modeled as riding. In **Ic**, most hydrogens were initially found in difference maps, but some of the solvent hydrogens were placed at geometrically plausible hydrogen bonding positions and treated as riding. For the riding models, standard low-temperature distances were applied [0.95 Å ($C_{sp2}H$), 0.99 Å (R_2CH_2), 1.00 Å (R_3CH), 0.88 Å ($N_{sp2}H$), and 0.84 Å (OH)]. In all cases hydrogen atom U_{iso} values were tied to their parent atom U_{eq} values (1.5U_{eq} for OH and CH_3, 1.2U_{eq} for all others). Crystal data, data collection, and experimental details for **Ia**, **Ib**, and **Ic** are summarized in Table 1.

2.4. Powder Diffraction. Nonsolvated crystals of **I** were ground with a small agate mortar and pestle. A small pellet (~0.2 mm diameter) of compressed powder was held in a fine polymer loop by a thin film of light polyisobutene oil. Two-dimensional (2-D) powder diffraction frames were collected on the same Bruker-Nonius X8 Proteum diffractometer used for single-crystal studies of **Ia** and **Ic**, but using the finest aperture beam-tunnel available. Data collection frames consisted of 360° rotation about the ϕ axis for 300 s at RT. Frames were radially integrated using DataSqueeze[26] or PhaseID within APEX2.[21] Calculated diffraction patterns based on the single-crystal structures of **Ia** and **Ib** were obtained using CrystalDiffract from the CrystalMaker suite.[27] For ease of comparison, calculated powder peaks were broadened to approximate the width of the experimental powder diffraction peaks.

2.5. Computational Details. Conformational energies for **I** in 5° increments of torsion angle about the glycosidic bond between purine and deoxyribose moieties, and for the iodine relative to deoxyribose were calculated using the NWChem software package.[28] The torsion angle in question was fixed and the geometry was allowed to relax for each angle using the B3LYP functional.[29,30] Cohesive energies between planes of iodine atoms in adjacent layers were calculated for the layer interfaces present in **Ia** and **Ib** using NWChem, with a dispersion corrected functional (B3LYP-D3).[31] Pairwise interaction energy decomposition analysis (PIEDA)[32] was performed using the GAMESS-US software package,[33] with the MP2 method.[34] To perform the calculations efficiently, while still properly describing the high number of electrons around iodine, two basis sets were employed at the same time. The lighter atoms, C, H, N, and O used the 6-31G* basis set, while iodine used the larger 6-311G* basis set.

3. RESULTS

3.1. General Structural Features of 5′-Deoxy-5′-iodoguanosine (I). Bond parameters for individual crystallographic models of **I** are largely unremarkable. The guanosine skeleton consists of two relatively rigid groups: a flat purine ring system and a deoxyribose ring with envelope geometry. The overall conformation of the molecule is determined by rotation about the glycosidic bond (N9−C1′), which orients the ring systems relative to each other. A less dramatic conformational degree of freedom consists in rotation about C4′−C5′, which defines the torsion of the iodine substituent at the C5′ position. Variation in puckering[35] of the deoxyribose ring is also possible. The molecule contains several potential strong hydrogen-bond donors and acceptors on both deoxyribose and purine moieties, so it is not surprising that major features of the crystal packing in both solvent-free and solvated forms are determined by hydrogen-bonding interactions.

3.2. Major Polymorph (Ia). The crystal used to refine the structure of polymorph **Ia** appeared to be solely **Ia**. The lath-shaped crystal was monoclinic, space group $P2_1$, with cell dimensions a = 7.6285(4) Å, b = 4.9951(2) Å, c = 16.1724(7) Å, β = 91.843(2)°. An ellipsoid plot is shown in Figure 1a. Deviation from planarity for the purine ring system is negligible (0.0105 Å). In the deoxyribose ring, the flap atoms (C2′, C3′, C4′) form a dihedral angle with the envelope atoms (C2′, C1′, O1′, C4′) of 37.0(3)°. The torsion angle (C8−N9−C1′−O1′) between the purine and deoxyribose rings is 28.5(7)°, while the torsions that define the iodine position [O1′−C4′−C5′−I1 = 61.2(5)° and C3′−C4′−C5′−I1 = 178.8(4)°] are *gauche* and *anti* respectively. Some conformational parameters are given in Table 2.

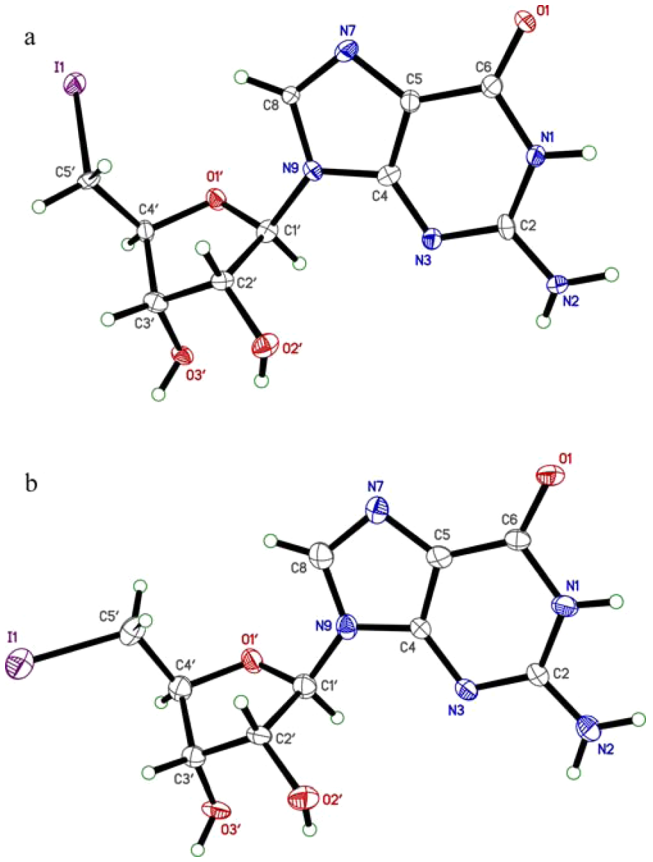

Figure 1. Ellipsoid plots (50% probability) of (a) polymorph **Ia** and (b) polymorph **1b**. In **Ia** the iodine is *gauche* relative to O1′ whereas in **Ib** it is *anti*.

In the crystal, all hydrogen bonding is intermolecular. A series of $R_2^2(10)$ motifs join the hydroxyl groups of the deoxyribose moiety to the purine of a translationally (1 + x, 1+ y, z) equivalent molecule into chains parallel to (110) by O−H···N and O−H···$O_{C=O}$ hydrogen bonds. The carbonyl oxygen is also involved as a bifurcated acceptor in an $R_2^1(6)$ motif involving the ring NH and one hydrogen (H1N2) of the exocyclic NH_2 group of a molecule related by the 2_1 screw axis parallel to b. This same exocyclic NH_2 donor hydrogen (i.e., H1N2) is bifurcated: it also interacts with O2′ of a 2_1 screw-related molecule (via 1 − x, −0.5 + y, 1 − z). Crystal packing for **Ia** is shown in Figure 2a, and hydrogen bond parameters are listed in Table 3. There are no π−π overlaps between purines on adjacent molecules. The dihedral angle between purine rings related by the 2_1 screw axis within one unit cell (i.e., via 1 − x, −0.5 + y, 1 − z) is 78.88(8)°. The net result of these strong hydrogen-bonding interactions are double layers of molecules that extend in the *ab* plane. These double-layered planes have exposed iodine atoms at the double-layer surfaces. In **Ia** the C5′−I1 bond is oriented such that the iodine atom protrudes *outside* the unit cell box and is 0.4258(3) Å from the *ab* plane, leading to a corrugated interface at which iodine atoms on adjacent double layers interdigitate (Figure 3a).

DOI: 10.1021/acs.cgd.6b00981
Cryst. Growth Des. 2016, 16, 6343−6353

Table 2. Conformation-Defining Torsion Angles (deg) and Deoxyribose Ring Puckering Parameters for Polymorphs Ia and Ib, and for the Mixed Water/Methanol Solvate Ic

	Ia	Ib	Ic_a	Ic_b
C4−N9−C1′−O1′ (deg)	−152.4(5)	−151(2)	−154.1(7)	−76.2(9)
C8−N9−C1′−O1′ (deg)	28.5(7)	33(3)	38.0(11)	100.8(9)
O1′−C4′−C5′−I1′ (deg)	61.2(5)	168.8(11)	174.9(5)	−54.8(9)
C3′−C4′−C5′−I1′ (deg)	178.8(4)	−76.8(19)	−66.8(9)	66.2(9)
Cremer−Pople Q (Å)	0.384(6)	0.37(2)	0.405(9)	0.397(9)
Cremer−Pople Φ (deg)	93.1(8)	100(3)	83.6(11)	268.2(12)

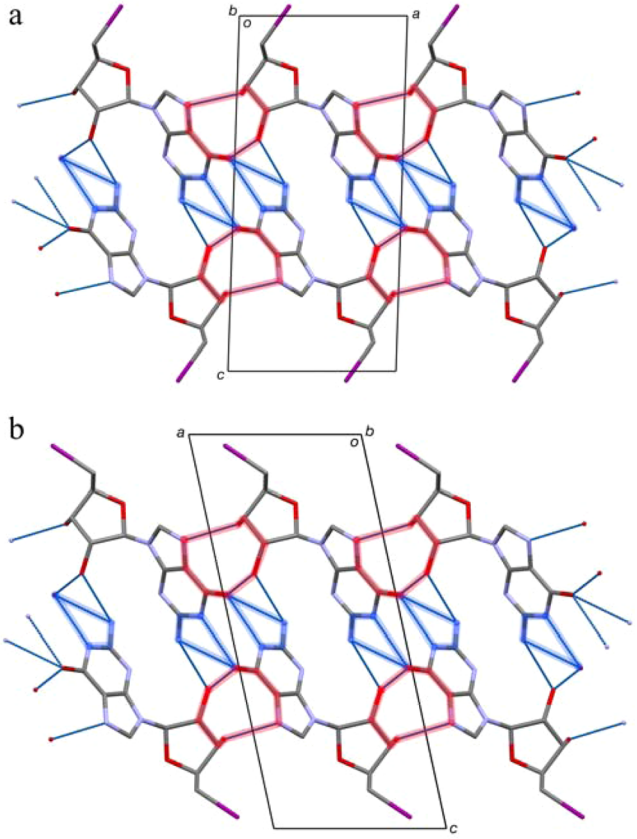

Figure 2. Crystal packing in (a) **Ia** and (b) **Ib** viewed as a projection onto the *ac* plane. Hydrogen bonding patterns in the double layers (thin blue lines) are ostensibly the same, which highlights the compatibility of the two polymorphs for epitaxial intergrowth. The $R_2^2(10)$ and $R_2^1(6)$ ring motifs are highlighted by thick semitransparent red and blue lines, respectively. The only substantial difference is the orientation of the iodine atoms (purple) at the top (*gauche*) and bottom (*anti*) of each image.

3.3. Minor Polymorph Ib. The crystal used to refine the structure of **Ib** was an epitaxially intergrown hybrid of polymorphs **Ia** and **Ib**. The structure is monoclinic, space group $P2_1$, with cell dimensions a = 7.5536 (15) Å, b = 4.9860(8) Å, c = 17.691(3) Å, β = 102.172(12)°. An ellipsoid plot of **Ib** is shown in Figure 1b. Bond lengths and angles are similar to the equivalent bonds in polymorph **Ia**, but are less precise because of the necessary deconvolution of overlapping reflections during data integration.[21] The geometry of the guanosine moiety is very similar to that in **Ia** [torsion angle (C8−N9−C1′−O1′) = 33(3)°], but the (O1′−C4′−C5′−I1) and (C3′−C4′−C5′−I1) torsions of 168.8(11)° and −76.8(19)° define *anti* and (suboptimal) *gauche* conformations

Table 3. Hydrogen Bonding in Polymorphs Ia and Ib

polymorph **Ia**	$d_{D\cdots H}$ (Å)	$d_{H\cdots A}$ (Å)	$d_{D\cdots A}$ (Å)	∠DHA (deg)
N1−H1···O1^{ia}	0.88	2.03	2.845(6)	153.1
N2−H1N2···O1^{ia}	0.82(5)	2.28(6)	3.001(7)	147(8)
N2−H1N2···O2′^{iia}	0.82(5)	2.37(8)	2.944(8)	127(8)
N2−H2N2···N3^{iia}	0.82(5)	2.46(6)	3.151(9)	143(7)
O2′−H2′1···O1^{iiia}	0.84	2.04	2.811(6)	151.3
O3′−H3′1···N7^{iiia}	0.84	1.98	2.774(6)	158.5

Symmetry codes: *ia* = (−*x* + 2, *y* − 1/2, −*z* + 1), *iia* = (−*x* + 1, *y* − 1/2, −*z* + 1), *iiia* = (*x* − 1, *y* − 1, *z*)

polymorph (**Ib**)	$d_{D\cdots H}$ (Å)	$d_{H\cdots A}$ (Å)	$d_{D\cdots A}$ (Å)	∠DHA (deg)
N1−H1···O1^{ib}	0.88	2.04	2.83(2)	149
N2−H1N2···O1^{ib}	0.88	2.34	3.14(2)	151.1
N2−H1N2···O2′^{iib}	0.88	2.22	2.98(2)	144.1
N2−H2N2···N3^{iib}	0.88	2.44	3.03(2)	125.1
O2′−H2′1···O1^{iiib}	0.84	2.02	2.77(2)	148.5
O3′−H3′1···N7^{iiib}	0.84	1.95	2.75(2)	158.2

Symmetry codes: *ib* = (−*x*, *y* + 1/2, −*z* + 1), *iib* = (−*x* + 1, *y* + 1/2, −*z* + 1), *iiib* = (*x* + 1, *y* + 1, *z*)

respectively, for the iodine substituent, i.e., opposite to **Ia**. Conformation defining parameters for **Ib** are given in Table 2.

Hydrogen bonding in **Ib** is virtually identical to that in **Ia**. The same graph-set motifs are present (Figure 2b) with just a few minor differences in geometric parameters, which are given in Table 3. The dihedral angle between purine rings related by the 2_1 screw axis within one unit cell [i.e., via (1 − *x*, 1/2 + *y*, 1 − *z*)] is 77.8(3)°, similar to **Ia**. The main differences arise from consequences of the conformations of the iodine substituents. In **Ib**, the iodine atom is 0.5187(12) Å from the *ab* plane on the *inside* of the unit cell box. This leads to a much less corrugated interface with no opportunity for iodines on adjacent double layers to interdigitate (Figure 3b).

3.4. Water/Methanol Solvate (Ic). Crystals of the water/methanol solvate are orthorhombic, space group $P2_12_12_1$, with cell dimensions a = 9.2724(2) Å, b = 10.5929(3) Å, c = 32.2592(8) Å. The asymmetric unit for **Ic** contains two independent molecules, Ic_a and Ic_b, and is shown in Figure 4.

As with the solvent-free structures, there are no unusual bond lengths or angles. The conformations of **I** in Ic_a and Ic_b, however, are quite different from each other, and from **Ia**, though Ic_a is similar to **Ib**. An overlay of the four conformations is shown in Figure 5. For Ic_a, the torsion between purine and deoxyribose moieties is 38.0(11)°, whereas in Ic_b it is 100.8(9)°. The torsion of the iodine substituent relative to the ring oxygen of deoxyribose in Ic_a is *anti* [174.9(5)°], whereas that of Ic_b is *gauche* [−54.8(9)°], but in the opposite sense to that of **Ib**. Conformational parameters are summarized in Table 2. The incorporated solvent consists of an ordered methanol, three relatively well-ordered waters and an ill-defined elongated blob of electron density located in small regions

DOI: 10.1021/acs.cgd.6b00981
Cryst. Growth Des. 2016, 16, 6343−6353

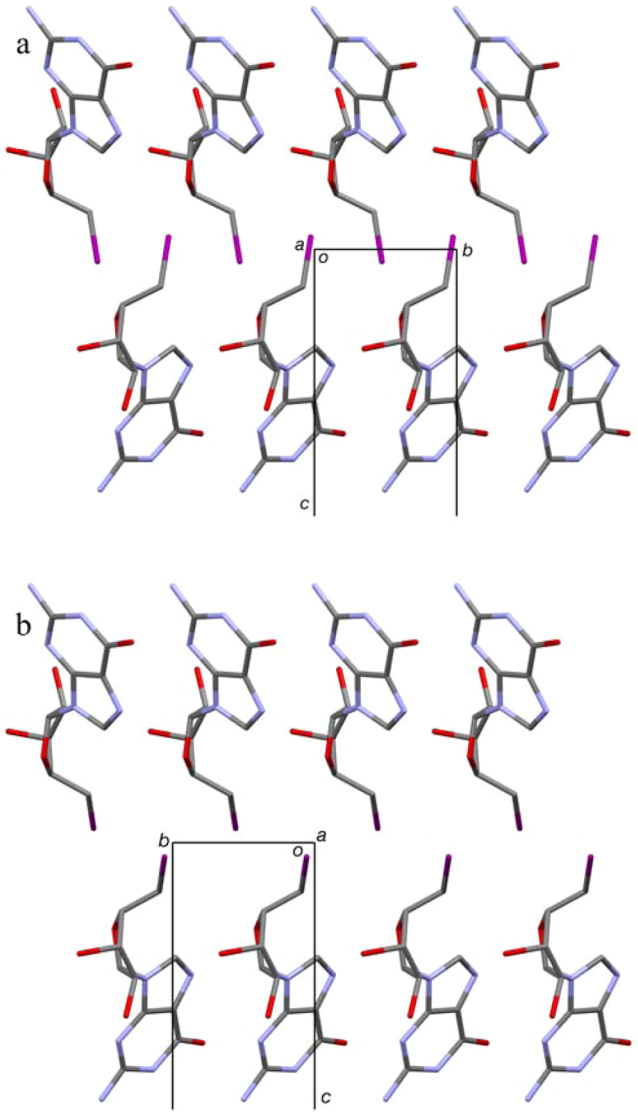

Figure 3. Interlayer packing in (a) **Ia** and (b) **Ib** viewed along *a* and −*a* of the respective crystal structures. In **Ia**, layers of *gauche*-oriented iodine substituents interdigitate, whereas in **Ib** the *anti*-oriented layers of iodines abut each other. The relative I···I contact area is thus much greater in **Ia** than in **Ib**.

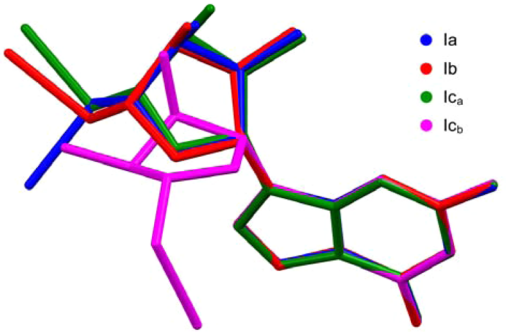

Figure 5. An overlay of the four experimentally determined conformations of **I**, based on a least-squares fit of atoms in the purine ring system. The conformations in polymorphs **Ia** and **Ib** differ primarily in the torsion of the iodine atom (far left). One conformation in the solvated crystals **Ic**$_a$ is very similar to that of polymorph **Ib**, while in the other, **Ic**$_b$, the deoxyribose ring position is substantially different.

between molecules **Ic**$_a$ and **Ic**$_b$ near the middle of the unit cell. We tried many different ways to model this feature, including various composites of disordered water, methanol, and mixtures of the two, none of which were truly satisfactory. Use of the SQUEEZE routine in Platon[36] to factor out this diffuse electron density was no better than a partial occupancy disordered solvent model. We settled with a composite of methanol and water (without hydrogen atoms), though its actual composition remains unknown. This has little bearing on the overall structure.

Hydrogen bonding within the solvate is considerably more complicated than **Ia** or **Ib** as it involves all the solvent molecules in addition to **I**. There are, however, several easily recognizable graph-set motifs: an $R_2^2(8)$ ring joins inequivalent purines in the same asymmetric unit by pairs of N−H···O hydrogen bonds; an $R_2^2(8)$ ring joins inequivalent purines in adjacent asymmetric units (via *x*, 1+ *y*, *z*) by pairs of long N−H···N hydrogen bonds; an $R^3{}_3(8)$ ring involves the carbonyl (as a bifurcated acceptor) and exocyclic amine of an inequivalent purine moiety (same asymmetric unit), and a water molecule; an $R_1^1(6)$ ring between inequivalent deoxyribose moieties related via the 2_1 screw axis along *b*. The dihedral angle between purine moieties within one asymmetric unit is 2.4(2)°, so the propagation of both sets of $R_2^2(8)$ motifs join the main molecules into gently undulating ribbons that extend parallel to *b*. Adjacent ribbons (via 1 − *x*, 0.5 + *y*, 0.5 − *z*) *π*−*π* stack

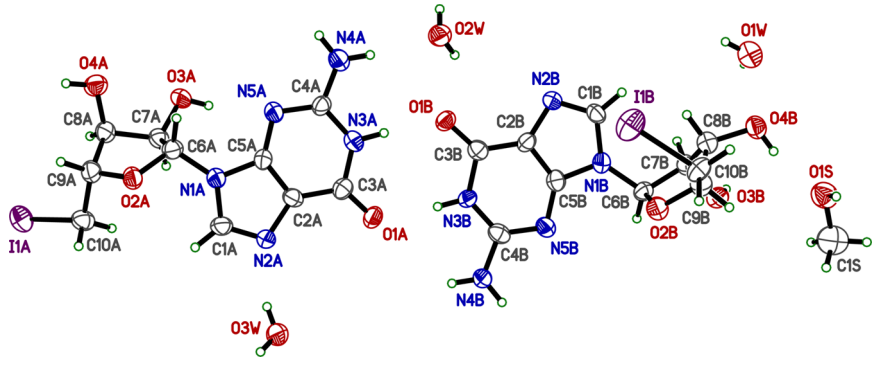

Figure 4. An ellipsoid plot (50% probability) of **Ic**. The conformations of the two molecules in the asymmetric unit **Ic**$_a$ on the left and **Ic**$_b$ on the right are quite different. A poorly defined feature that was modeled as a disordered superposition of partial occupancy water and methanol is omitted to improve clarity.

DOI: 10.1021/acs.cgd.6b00981
Cryst. Growth Des. 2016, 16, 6343−6353

between the five- and six-membered rings of symmetry inequivalent pairs of purine moieties, with layer spacing 3.330(19) Å. These stacked bilayers of ribbons are built into an extended three-dimensional (3-D) structure by a complex network of O−H···N, N−H···O, and O−H···O hydrogen bonds (see SI Table S1 and Figure S2) involving the main molecules, water, methanol, and the poorly defined disordered feature mentioned above.

3.5. Unusual Single-Crystal Diffraction from Solvent-Free I. Most crystals of solvent-free **I** were laths (SI, Figure S1) that gave diffraction patterns that indexed as **Ia**. Some crystals gave diffraction patterns showing a single reciprocal lattice corresponding to **Ia**, but many others had faint additional reflections. These were consistently along c^* only, but had intensities that varied from crystal to crystal. Crystals that had been kept wet for ∼3 years were all laths and seemed to be exclusively **Ia** (see section 3.6 and SI Figure S3). A very small number of dried crystals were semiregular squat slabs, one of which gave diffraction showing two reciprocal lattices that had diffraction spots with similar relative intensities. We did not find any crystals that were single-component **Ib**. Reconstructed diffraction images showing slices of reciprocal space in the ($0kl$) plane for a lath-shaped crystal (UK data) and for a squat slab (ALS data) are shown in Figure 6. For the lath, reflections from the main lattice are clearly dominant, but there are additional weak Bragg peaks between some of the main reflections along c^*. For the slab, the "extra" reflections are considerably more intense. We initially suspected twinning, but these extra reflections could not be accounted for using any twin law. Temperature variation between 90 K and ∼250 K had little discernible effect on the relative intensities of the "extra" reflections. Attempts to interpret them as modulation-induced satellite peaks were futile. For data from solvent-free crystals that had such extra reflections, difference Fourier maps sometimes gave small but non-negligible (∼1−2 e·Å^{-3}) peaks at a position well removed from the iodine atom in **Ia**. While this "ghost" peak could be interpreted as a minor disorder component for the iodine, such a disorder model does nothing to explain the presence of the extra reflections. In spite of the fact that all crystals gave sharp extinctions when rotated between crossed polarizers, the likelihood that these were hybrid crystals containing a variable amount of an unknown phase was compelling. At the ALS, this second phase indexed as **Ib** with a unit cell volume [651.3(2) Å^3] that is significantly larger than that of **Ia** [615.95(5) Å^3]. We suspected that **Ib** might be an epitaxially intergrown hydrate, similar to some uric acid crystals,[19,20] but subsequent analysis proved it to be a true second polymorph.

3.6. Powder Diffraction from Solvent-Free I. Experimental powder diffraction patterns obtained from a bulk sample of pulverized crystals (Figure 7) gave a series of peaks that correspond very closely to peaks in a simulated powder pattern calculated from the crystal structure of **Ia**. A few small peaks, however, did not match up, and these anomalous peaks were reproducible across powders prepared from different batches of solvent-free crystals. A simulated powder pattern calculated from the crystal structure of **Ib**, however, readily explains these features. As with the single-crystal data, it is clear from these powder patterns that **Ia** is by far the dominant polymorph. A powder pattern from wet crystals that had sat undisturbed for ∼3 years showed virtually no **Ib** (see SI Figure S4). There was no evidence of the mixed solvate form **Ic** in any experimental powder patterns.

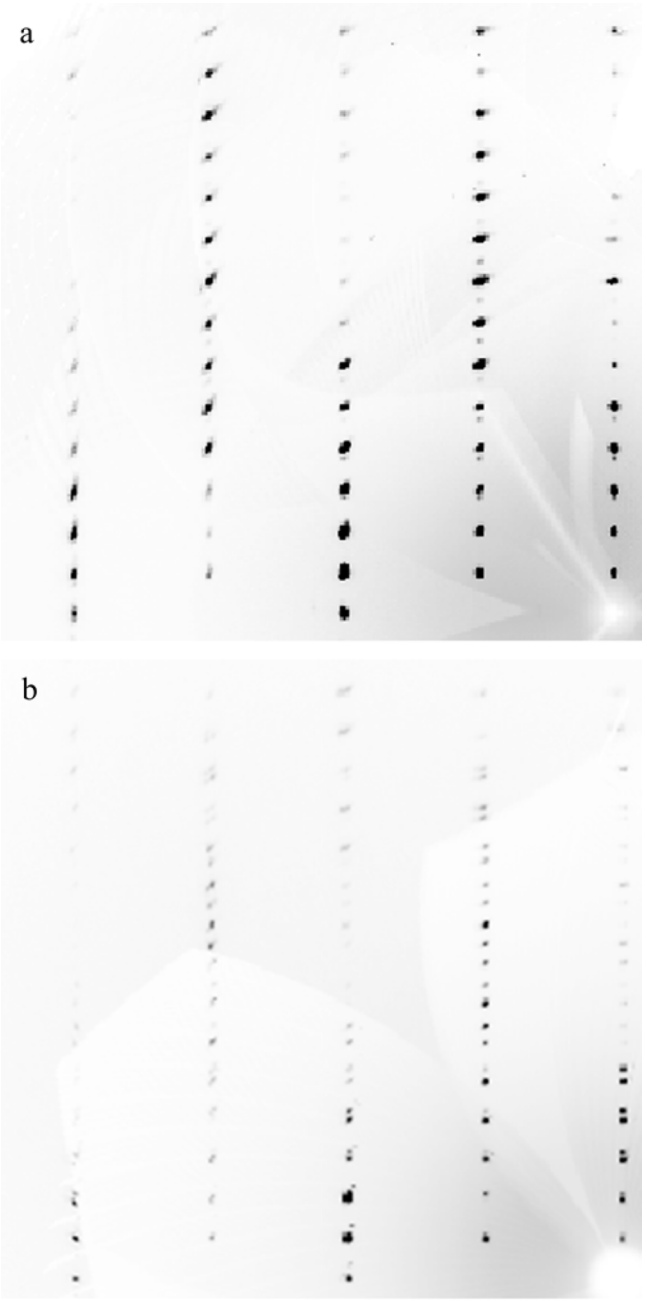

Figure 6. Reciprocal-space-slice images reconstructed from a full set of diffraction frames for (a) lath-shaped and (b) slab-shaped crystals of solvent-free **I**, each showing the presence of two reciprocal lattices. In (a) reflections from one lattice are clearly dominant, whereas in (b) neither appears to be dominant.

3.7. Computational Modeling. A series of electronic structure calculations were performed to determine the influence of conformation on the different packing arrangements. DFT energies of the isolated molecules, using coordinates taken directly from the respective crystal structures, but with allowance for the hydrogen atoms to "relax" from their foreshortened X-ray crystal structure distances[39] reveal the conformation in **Ia** to be less stable than that in **Ib** by ∼1.5 kcal/mol. On isolated molecules, the effect of torsional angle variation (i.e., about the N9−C1′ and C4′−C5′ bonds) was investigated through a series of geometry optimizations. The dihedral angle in question was fixed at the desired angle, while

DOI: 10.1021/acs.cgd.6b00981
Cryst. Growth Des. 2016, 16, 6343−6353

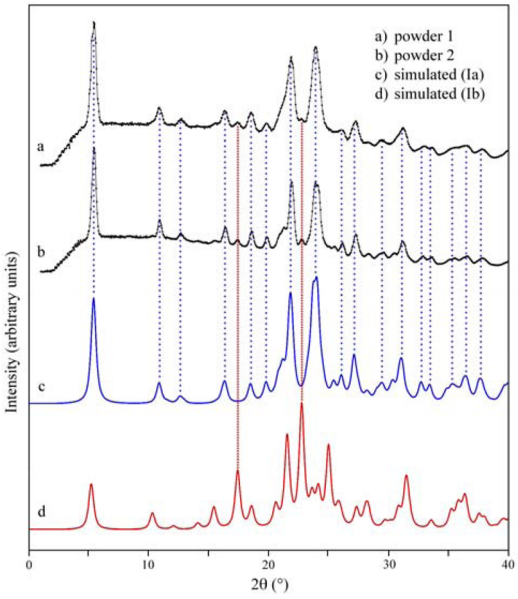

Figure 7. Qualitative comparison of powder diffraction patterns for solvent-free **I**. The black traces, (a) and (b), are experimental patterns from two different batches of crystals. The blue (c) and red (d) traces are simulated patterns calculated from the refined crystal structures of **Ia** and **Ib** respectively. The blue dotted vertical lines show the match up between experimental powder lines and those calculated from the crystal structure of **Ia**. The red vertical lines show the match up of two small features in the experimental powder patterns with peaks calculated from the crystal structure of **Ib**.

the rest of the molecule was allowed to relax. The angle was varied from −180° to +180° in 5° increments. Two optimizations were performed for each torsion, one based on the starting geometry of form **Ia** and the other starting from **Ib**.

3.7.1. Torsion about the Glycosidic Bond between Purine and Deoxyribose. For the deoxyribose−purine bond (i.e., torsion C4−N9−C1′−O1′), minimum energies were found for torsion angles of 75° and 175° when using the initial geometry of **Ia** (Figure 8). Starting from the molecular geometry of **Ib**, however, gives deeper potential wells for this torsion, with minima at −120° and 75°: the corresponding torsion angles in the crystal structures of **Ia** and **Ib** are −152.4(5)° and −151(2)°, respectively (Table 2). The mismatch here between crystal structures and optimized isolated molecule conformations is due to the extensive intermolecular hydrogen-bonding network in the crystals. The implication, however, is that relaxation about the N9−C1′ bond leads to lower conformational energy if the iodine atom is placed as in **Ib** versus that in **Ia**.

3.7.2. Torsion of Iodine Relative to Deoxyribose. The torsion of the iodine relative to the ring oxygen of the deoxyribose group (i.e., I1−C5′−C4′−O1′) was investigated in a similar manner, yielding a minimum at 65° when starting from geometry **Ia** (Figure 9). Other local minima were found at −65° and 170°, both being around 1 kcal/mol higher in energy than the global minimum. The barrier for rotation for this bond was found to be around 6−8 kcal/mol. Starting from geometry **Ib**, the minimum at 65° is destabilized, while the minima at −65° and 175° become more stable, with the latter becoming the global minimum (Figure 9). There is good agreement between these optimized torsion angles and those measured in the crystal structures [61.2(5)° and 168.8(11)° respectively],

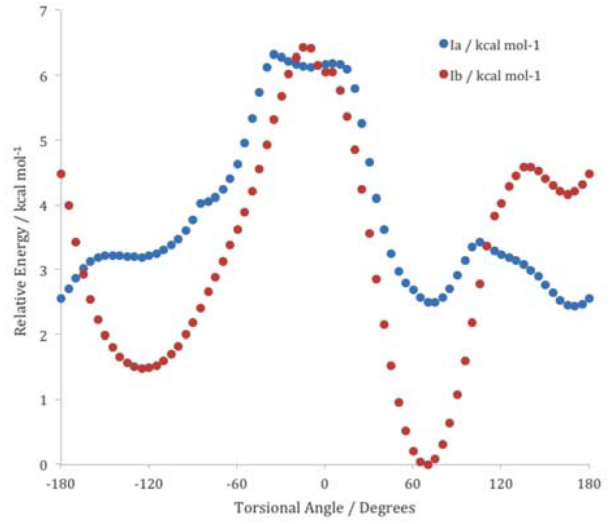

Figure 8. Isolated-molecule conformational energies for torsion (C4−N9−C1′−O1′) around the purine-deoxyribose groups starting from the experimental geometries of **Ia** and **Ib**. The **Ib** conformation is able to relax to a lower-energy geometry than the **Ia** conformation.

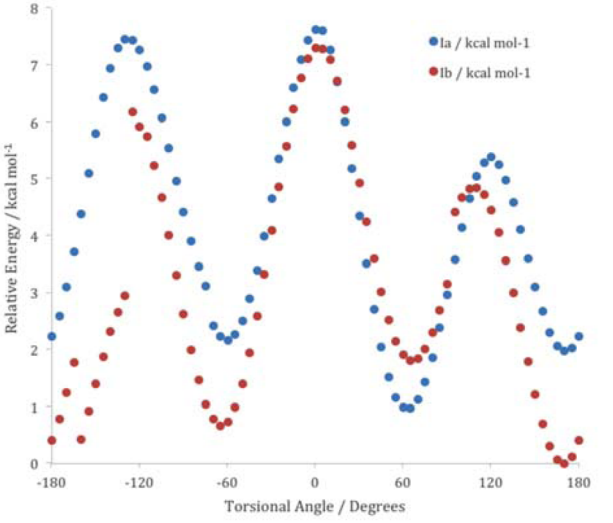

Figure 9. Isolated-molecule conformational energies for torsion (I1−C5′−C4′−O1′) of the iodine relative to the deoxyribose group. The lowest energy conformer occurs at 175° when the starting model is **Ib** and is ∼1 kcal/mol lower than the lowest energy conformer (∼65°) when starting from **Ia**. For **Ib**, the trace is offset to lower energy by ∼3 kcal/mol between about −130° and −160°: an effect caused by a change in the puckering of the deoxyribose ring. Computed geometries at each of the minima are shown in SI Figure S5.

while the two rotational degrees of freedom are shown to be dependent on one another. In the conformational analysis summarized in Figure 9, the torsions between about −130° and −160° for the **Ib** starting model are offset to lower energy by ∼3 kcal/mol. This unusual feature is due to an unexpected rearrangement of the deoxyribose ring conformation for the optimized structures. Interestingly, a similar rearrangement of the deoxyribose ring is evident in molecule $\mathbf{Ic}_b$ of the mixed solvate (Table 2), albeit at different angles.

*3.7.3. Cohesive Energies between Layers of Molecules in Polymorphs **Ia** and **Ib**.* To investigate the differences in

DOI: 10.1021/acs.cgd.6b00981
Cryst. Growth Des. 2016, 16, 6343−6353

packing between **Ia** and **Ib**, specifically at the iodine−iodine layer interfaces, the interactions between molecules were calculated using a supermolecular approach. The energy of a pair of molecules (Figure 10) taken directly from the crystal

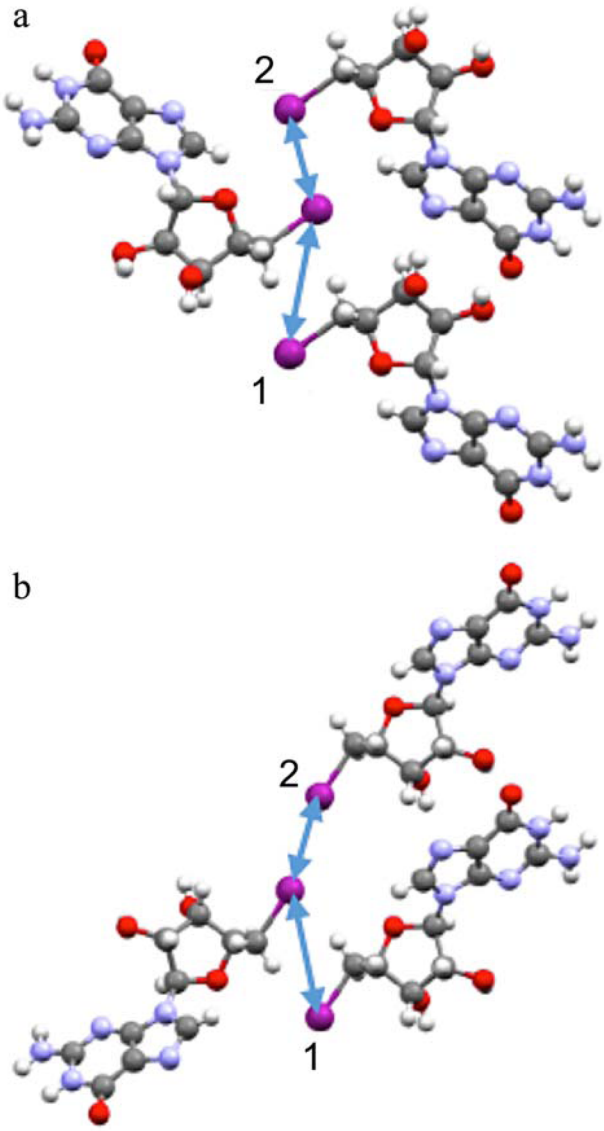

Figure 10. Pairs of molecules used to define iodine-involving interactions in (a) polymorph **Ia** and (b) polymorph **Ib** for pairwise interaction energy calculations. The structure fragments were taken directly from the refined crystal structures, and the hydrogen positions were allowed to relax.

structure was calculated after allowing hydrogen atoms to relax,[39] using a dispersion-corrected DFT functional to properly describe the stabilizing dispersion intermolecular forces. In addition to calculating the energy of the dimer, the energies of isolated individual molecules were calculated at the same computational level. The interaction energy, E_{int}, is given by the difference between the dimer and the sum of its isolated components. The interaction between layers in the *c*-direction involving iodine atoms was investigated through pairwise interactions, as well as the overall interaction between one molecule and its four nearest neighbors (Table 4). Both uncorrected and counterpoise corrected (to account for basis set superposition error) values are reported. The interdigitation in form **Ia** clearly leads to a more favorable interaction energy over form **Ib** due to closer intermolecular distances. The interaction energies obtained in the cluster approach do not completely match the sum of the pairwise interactions, where the electron density can be distributed to maximize the interaction between one pair, without decreasing an adjacent interaction, but are in fairly good agreement.

To describe the interactions in more detail, we used pairwise interaction energy decomposition analysis (PIEDA)[32] to break down the overall interaction energy into separate electrostatic, exchange, charge transfer, and dispersion terms. The electrostatic energy is due to interactions of permanent partial charges on both molecules, while the charge transfer energy is due to the charge on one molecule inducing a temporary dipole on the second molecule. The exchange energy is the electron−electron repulsion between molecules, while the movement of electrons due to the above terms leads to temporary dipoles on both molecules, leading to the dispersion term. The PIEDA calculations were run on molecular pairs (vide supra, Figure 10) taken directly from the crystal structures, using the Møller−Plesset MP2 method and the same mixed basis sets as before. Once again, the interdigitating iodines give a stronger total interaction energy (Figure 11). In most of the pairs, the major stabilizing factor is dispersion, which is counteracted by the exchange repulsion. Electrostatic stabilization is also sizable. The exception is pair 1 of **Ia**, which shows a stronger electrostatic than dispersion energy. The minimal number of close contacts in **Ib** pair 2 results in overall weak interactions. Comparing these results with measurement of close intermolecular contacts in each pair (see SI Table S2 for details), we can postulate that the increased electrostatic stabilization in **Ia-1** may come from multiple close I···H interactions. Meanwhile, in addition to the stabilizing effects of halogen bonding[37] and interhalogen interactions,[38] interactions between electron rich atoms (I···I and I···O) contribute to stabilization by both dispersion and electrostatics observed in the PIEDA analysis of **Ia-2**.

4. DISCUSSION

4.1. Differences in Habit of Solvent-Free Crystals of (I). The vast majority of hybrid crystals were lath shaped, but a very small number were squat slabs. What could cause the observed differences in crystal shape? There are two obvious

Table 4. Pairwise and Cluster Interaction Energies between Closest Neighboring Molecules with Interactions Involving Iodine

	B3LYP-D3 interaction energies[a] in kcal/mol			
	pair 1[b]	pair 2	sum of all closest pairs	cluster
Ia	−8.05 (−7.32)	−4.88 (−3.18)	−25.86 (−21.0)	−23.73 (−19.48)
Ib	−4.97 (−4.10)	−1.60 (−1.41)	−13.14 (−11.02)	−12.97 (−11.06)

[a]Numbers in parentheses used counterpoise correction to account for the basis set superposition error. [b]Specific molecule pairs are defined in Figure 10.

DOI: 10.1021/acs.cgd.6b00981
Cryst. Growth Des. 2016, 16, 6343−6353

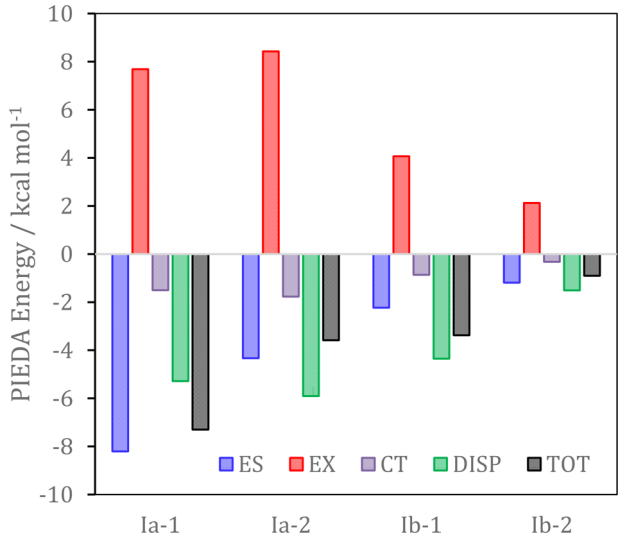

Figure 11. MP2 Pairwise interaction energy decomposition analysis for close contacts between iodine-containing groups of adjacent molecules, after hydrogen relaxation. ES = electrostatic, EX = exchange, CT = charge transfer, DISP = dispersion, TOT = total interaction energy.

possibilities: either the squat slab was a fragment broken from a lath, or the presence of **Ib** impeded crystal growth, especially along *b*, thereby foreshortening the laths into slabs. The latter explanation is more attractive for several reasons. It is clear from Figure 6 that the laths contain considerably less **Ib** than the sole slab-shaped crystal that we analyzed in detail. On the basis of comparison of relative reflection intensities, a rough estimate for the fraction of **Ib** in typical lath-shaped crystals is 0−2%, while for the squat slab it was closer to 50%. Moreover, the squat slab did not *look* like a broken piece of lath. At the ALS, the squat slab was selected precisely because it looked so different from the rest of the crystals. Besides, if it were simply a fragment broken from a lath, it ought to have had a similar **Ib** content to the other laths that were analyzed in detail.

4.2. Compatibility of Unit Cells for Ia and Ib. The compatibility of hydrogen-bonding networks (Figure 2) and the incompatibility of iodine-containing layers (Figure 3) suggest that the interface between conjoined polymorphs consists of a hybrid double layer in the *ab* plane, composed of a layer of **Ia** hydrogen bonding with a layer of **Ib**. Epitaxy solely in the *ab* plane agrees with the evidence from diffraction: all "extra" reflections (e.g., Figure 6) occur along directions parallel to *c**, which is perpendicular to the *ab* plane. The *a*-axis and *b*-axis lengths of **Ia** are ∼1% and ∼0.2% longer than those of **Ib**, leading to a mismatch of ∼1% for the areas of the *ab* faces of **Ia** and **Ib**. While these differences are small, the cumulative effect over several repeat distances rapidly lead to a substantial discrepancy (Figure 12), which could plausibly poison the growing crystal surface, thereby impeding crystal growth in the *a* and/or *b*-axis directions. This is consistent with the laths having a relatively low proportion of **Ib** and the squat slab having comparatively higher **Ib** content. The line of reasoning here is inspired by the crystal habit modification work of Leiserowitz and Lahav[40,41] in which "tailored" dopant molecules were shown to inhibit crystal growth in specific directions.

4.3. Conformational Energies and Implications for Crystal Growth. For isolated molecules, the computed overall conformation energy for **Ia** is higher than that of **Ib**. The iodine atom torsions with the deoxyribose ring can be defined relative to O1′ and to C3′. In **Ia**, the former is *gauche* and the latter is *anti*, while in **Ib** these assignments are reversed. In **Ia**, the angles (Table 2) are closer to ideal values than **Ib**, but "ideal values" make no account of the crystal-packing environment in the solid state. For isolated molecules, although conformational energies for the two torsional degrees of freedom are coupled, computed energies suggest a ∼1.5 kcal/mol advantage for the **Ib** conformer. This of course ignores neighboring molecules, and so need not be relevant in the crystal or even in solution. In the crystalline state, **Ia** is clearly dominant, which combined with its higher density (2.120 vs 2.005 Mg m^{-3} for **Ia** and **Ib** respectively) suggests it is thermodynamically more stable at room temperature. This makes intuitive sense given the striking difference in how the iodine layers interact in **Ia** vs **Ib**. Pairwise and cluster interaction energies for model layer fragments strongly favor the interdigitated **Ia** over the abutted **Ib**. What then to make of **Ib**? Since the *ab* layers are extensively hydrogen bonded in two directions it seems likely that fragments of such layers exist in solution. Such layers would be expected to look more like layers of **Ib** than **Ia** because the **Ib** form layers are ∼1.1% denser (*ab* = 37.66 vs 38.11 $Å^2$) and the molecules have a more favorable conformation. When such a fragment joins the growing crystal there would be a driving force for the $-CH_2I$ groups to "zip up" to give form **Ia**, but sometimes that process could fail, leading to domains of form **Ib**. In this scenario, **Ib** would be a metastable kinetic product.[42] Efficient conversion of **Ib** to **Ia** could thus be dependent on the presence of solvent, and at least for wet crystals, there was a tendency for the presence of **Ib** to diminish over time.

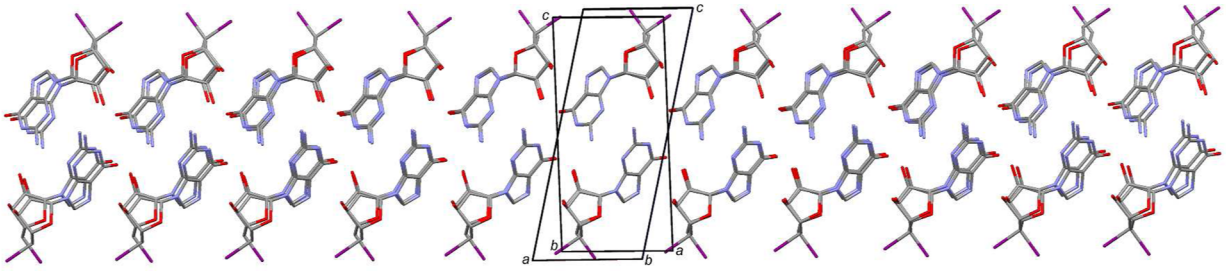

Figure 12. An overlay of 11 repeats along the *a*-axis for **Ia** and **Ib**, projected perpendicular to *ac*, based on a least-squares fit of atoms in the purine groups in the central pairs of overlaid molecules. The unit cells of **Ia** and **Ib** tilt to the left and right, respectively. The mismatch along the *a*-direction rapidly accumulates and could plausibly poison the surface, impeding growth in the *a* and/or *b*-directions, thereby foreshortening lath-shaped crystals into squat slabs for high **Ib** content crystals.

DOI: 10.1021/acs.cgd.6b00981
Cryst. Growth Des. 2016, 16, 6343−6353

5. SUMMARY

Solvent-free crystals of 5′-deoxy-5′-iodo guanosine coexist as hybrids of two conformational polymorphs that differ primarily in the orientation of the 5′-iodo substituent relative to the deoxyribose ring. The guanosine groups in each polymorph are in similar enough orientations to allow epitaxial intergrowth of the two forms. Although the more common polymorph could be obtained in essentially pure form, the less common polymorph was only found in hybrid crystals containing both polymorphs. Computational analysis suggests that for isolated molecules, the less common polymorph geometry is energetically more favorable. In the crystalline state, however, this leads to a much less favorable packing arrangement between layers of exposed iodine substituents. The implication is that the less common polymorph is a kinetic product, while the more common polymorph is the thermodynamically more stable crystalline form at room temperature.

■ ASSOCIATED CONTENT

Supporting Information

The Supporting Information is available free of charge on the ACS Publications website at DOI: 10.1021/acs.cgd.6b00981.

Figure S1. A photograph of typical lath-shaped crystals of **I**. Figure S2. A packing plot for the mixed solvate **Ic** viewed down the (a) *a* axis and (b) *b* axis. Figure S3. Reciprocal-space-slice images for the (0*kl*) and (*h*0*l*) layers for a solvent-free crystal that had aged in mother liquor for ∼3 years. Figure S4. Qualitative powder diffraction pattern for pulverized solvent-free crystal that had aged in mother liquor for ∼3 years. Figure S5. Computed geometries at the minimum points shown in Figure 9. Table S1. Hydrogen bond parameters for the mixed water/methanol solvate **Ic**. Table S2. Close-contact distances (Å) for different types of atom−atom interactions between pairs of molecules defined in Figure 10 of the main manuscript (PDF)

Accession Codes

CCDC 1486096−1486098 contain the supplementary crystallographic data for this paper. These data can be obtained free of charge via www.ccdc.cam.ac.uk/data_request/cif, or by emailing data_request@ccdc.cam.ac.uk, or by contacting The Cambridge Crystallographic Data Centre, 12 Union Road, Cambridge CB2 1EZ, UK; fax: +44 1223 336033.

■ AUTHOR INFORMATION

Corresponding Author

*Address: Department of Chemistry, University of Kentucky, 505 Rose Street, Lexington, KY, 40506-0055. E-mail: s.parkin@uky.edu.

Author Contributions

S.R.P. and K.J.G. performed crystallographic analyses, K.J.T. conducted quantum-chemical calculations, and E.J.B. was responsible for synthesis and crystal growth. The manuscript includes contributions from all authors, and all authors have given approval to the final version of the manuscript.

Notes

The authors declare no competing financial interest.

■ ACKNOWLEDGMENTS

We are grateful to Prof. Carolyn Brock for very useful discussions. The X8 Proteum at UK was funded by the NSF (MRI CHE-0319176). The Advanced Light Source is supported by the Director, Office of Science, Office of Basic Energy Sciences of the U.S. Department of Energy under Contract No. DE-AC02-05CH11231.

■ REFERENCES

(1) Buerger, M. J.; Bloom, M. C. *Z. Kristallogr. - Cryst. Mater.* **1937**, *96*, 182−200.
(2) McCrone, W. C. In *Physics and Chemistry of the Organic Solid State*; Fox, D., Labes, M. M., Weissberger, A., Eds. Interscience Publishers: New York, 1965; Vol. *2*, 725−767.
(3) Bernstein, J. *Polymorphism in Molecular Crystals*; Oxford University Press: Oxford, UK, 2002.
(4) Seddon, K. R. *Cryst. Growth Des.* **2004**, *4*, 1087.
(5) Desiraju, G. R. *Cryst. Growth Des.* **2004**, *4*, 1089−1090.
(6) Bernstein, J. *Cryst. Growth Des.* **2005**, *5*, 1661−1662.
(7) Bauer, J.; Spanton, S.; Henry, R.; Quick, J.; Dziki, W.; Porter, W.; Morris, J. *Pharm. Res.* **2001**, *18*, 859−866.
(8) Jurchescu, O. D.; Mourey, D. A.; Subramanian, S.; Parkin, S. R.; Vogel, B. M.; Anthony, J. E.; Jackson, T. N.; Gundlach, D. J. *Phys. Rev. B: Condens. Matter Mater. Phys.* **2009**, *80*, 085201.
(9) Diao, Y.; Chung, H. *J. Mater. Chem. C* **2016**, *4*, 3915−3933.
(10) Brear, P.; Freeman, G. R.; Shankey, M. C.; Trmčić, M.; Hodgson, D. R. W. *Chem. Commun.* **2009**, 4980−4981.
(11) Zhang, B.; Cui, Z.; Sun, L. *Org. Lett.* **2001**, *3*, 275−278.
(12) Fiammengo, R.; Musílek, K.; Jäschke, A. *J. Am. Chem. Soc.* **2005**, *127*, 9271−9276.
(13) Williamson, D.; Cann, M. J.; Hodgson, D. R. W. *Chem. Commun.* **2007**, 5096−5098.
(14) McGee, D. P. C.; Martin, J. C. *Can. J. Chem.* **1986**, *64*, 1885−1889.
(15) Kim, I.-H.; Shin, S.; Jeong, Y.-J.; Hah, S. S. *Tetrahedron Lett.* **2010**, *51*, 3446−3448.
(16) Lee, G. H.; Lim, H. K.; Hah, S. S. *Bull. Korean Chem. Soc.* **2011**, *32*, 3767−3769.
(17) Freer, S. T.; Kraut, J. *Acta Crystallogr.* **1965**, *19*, 992−1002.
(18) Bond, A. D.; Boese, R.; Desiraju, G. R. *Angew. Chem., Int. Ed.* **2007**, *46*, 618−622.
(19) Ringertz, H. *Acta Crystallogr.* **1966**, *20*, 397−403.
(20) Parkin, S.; Hope, H. *Acta Crystallogr., Sect. B: Struct. Sci.* **1998**, *54*, 339−344.
(21) *APEX2*; Bruker-AXS Inc.: Madison, WI, USA, 2006.
(22) Krause, L.; Herbst-Irmer, R.; Sheldrick, G. M.; Stalke, D. *J. Appl. Crystallogr.* **2015**, *48*, 3−10.
(23) Parkin, S.; Moezzi, B.; Hope, H. *J. Appl. Crystallogr.* **1995**, *28*, 53−56.
(24) Sheldrick, G. M. *Acta Crystallogr., Sect. A: Found. Adv.* **2015**, *71*, 3−8.
(25) Sheldrick, G. M. *Acta Crystallogr., Sect. C: Struct. Chem.* **2015**, *71*, 3−8.
(26) Heiney, P. *Commission on Powder Diffraction Newsletter* **2005**, *32*, 9−11.
(27) *CrystalDiffract*; CrystalMaker Software Ltd: Oxford, England.
(28) Valiev, M.; Bylaska, E. J.; Govind, N.; Kowalski, K.; Straatsma, T. P.; Van Dam, H. J. J.; Wang, D.; Nieplocha, J.; Apra, E.; Windus, T. L.; de Jong, W. A. *Comput. Phys. Commun.* **2010**, *181*, 1477−1489.
(29) Becke, A. D. *J. Chem. Phys.* **1993**, *98*, 5648−5652.
(30) Lee, C.; Yang, W.; Parr, R. G. *Phys. Rev. B: Condens. Matter Mater. Phys.* **1988**, *37*, 785−789.
(31) Grimme, S.; Antony, J.; Ehrlich, S.; Krieg, H. *J. Chem. Phys.* **2010**, *132*, 154104.
(32) Fedorov, D. G.; Kitaura, K. *J. Comput. Chem.* **2007**, *28*, 222−237.
(33) Schmidt, M. W.; Baldridge, K. K.; Boatz, J. A.; Elbert, S. T.; Gordon, M. S.; Jensen, J. H.; Koseki, S.; Matsunaga, N.; Nguyen, K. A.; Su, S.; Windus, T. L.; Dupuis, M.; Montgomery, J. A. *J. Comput. Chem.* **1993**, *14*, 1347−1363.

DOI: 10.1021/acs.cgd.6b00981
Cryst. Growth Des. 2016, 16, 6343−6353

(34) Head-Gordon, M.; Pople, J. A.; Frisch, M. J. *Chem. Phys. Lett.* **1988**, *153*, 503−506.
(35) Cremer, D.; Pople, J. A. *J. Am. Chem. Soc.* **1975**, *97*, 1354−1358.
(36) Spek, A. L. *Acta Crystallogr., Sect. D: Biol. Crystallogr.* **2009**, *65*, 148−155.
(37) Cavallo, G.; Metrangolo, P.; Milani, R.; Pilati, T.; Priimagi, A.; Resnati, G.; Terraneo, G. *Chem. Rev.* **2016**, *116*, 2478−2601.
(38) Saha, B. K.; Rather, S. A.; Saha, A. *Cryst. Growth Des.* **2016**, *16*, 3059−3062.
(39) Mitchell-Koch, K. R.; Matzger, A. J. *J. Pharm. Sci.* **2008**, *97*, 2121−2129.
(40) Berkovitch-Yellin, Z.; Addadi, L.; Idelson, M.; Lahav, M.; Leiserowitz, L. *Angew. Chem., Int. Ed. Engl.* **1982**, *21*, 1336−1345.
(41) Berkovitch-Yellin, Z.; van Mil, J.; Addadi, L.; Idelson, M.; Lahav, M.; Leiserowitz, L. J. *J. Am. Chem. Soc.* **1985**, *107*, 3111−3122.
(42) Steed, J. W. *CrystEngComm* **2003**, *5*, 169−179.

DOI: 10.1021/acs.cgd.6b00981
Cryst. Growth Des. 2016, 16, 6343−6353